Electronic Supplementary Information

Enhanced Detection Sensitivity on Chemisorption of Pyridine and Biotinylated Proteins at Localized Surface Plasmon Resonance Inflection Points in Single Gold Nanorods

Kyeong Rim Ryu[a] and Ji Won Ha[a,b*]

[a]Advanced Nano-Bio-Imaging and Spectroscopy Laboratory, Department of Chemistry, University of Ulsan, 93 Daehak-ro, Nam-gu, Ulsan 44610, Republic of Korea

[b]Energy Harvest-Storage Research Center (EHSRC), University of Ulsan, 93 Daehak-ro, Nam-gu, Ulsan 44610, Republic of Korea

[*]To whom correspondence should be addressed.

J. W. Ha

Phone: +82-52-712-8012

Fax: +82-52-712-8002

E-mail: jwha77@ulsan.ac.kr

This document contains supplementary figures (Figures S1 to S9).

Supplementary Figures

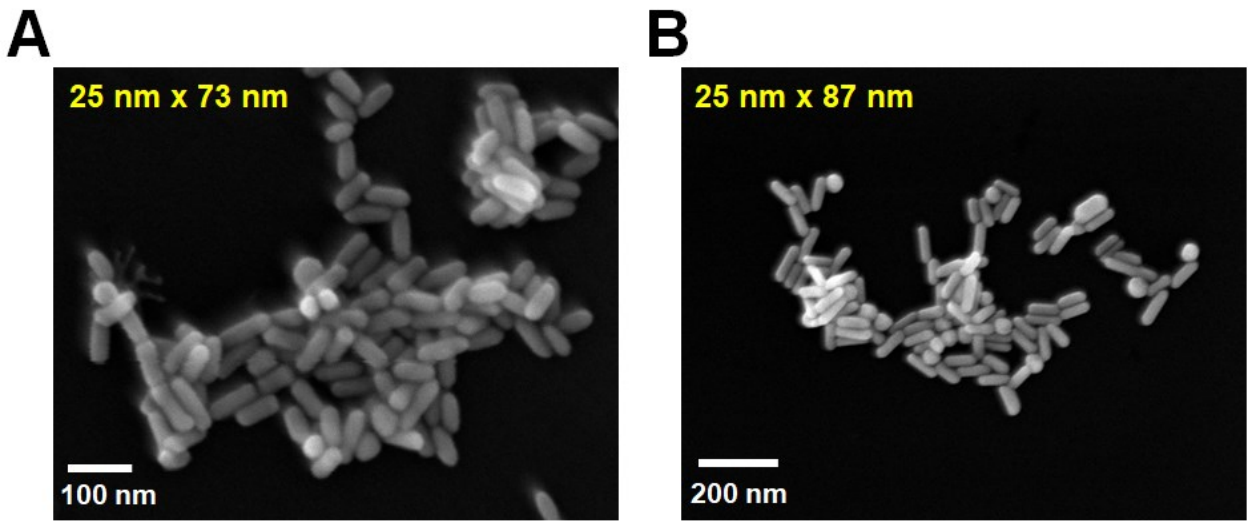

Fig. S1 (A) SEM image of AuNRs with an AR of 2.97 (25 nm × 73 nm). **(B)** SEM image of AuNRs with an AR of 3.48 (25 nm × 87 nm).

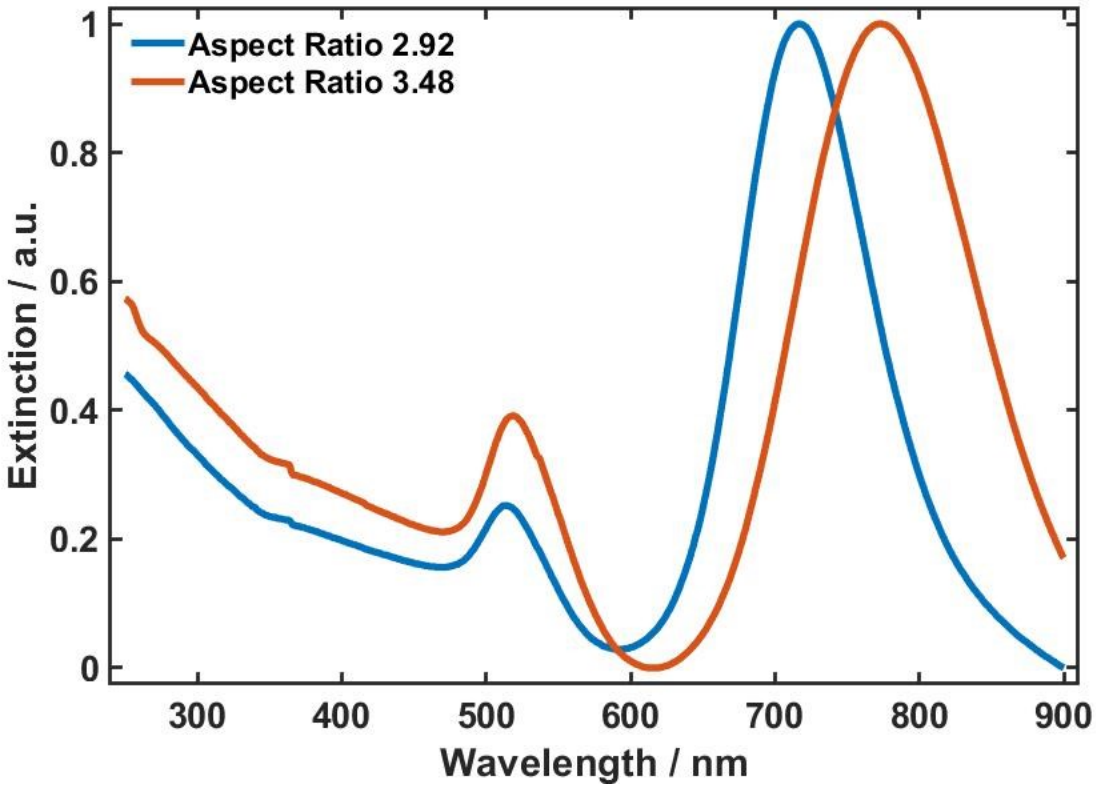

Fig. S2 Overlaid UV-Vis extinction spectra of AuNRs with two different ARs dispersed in water.

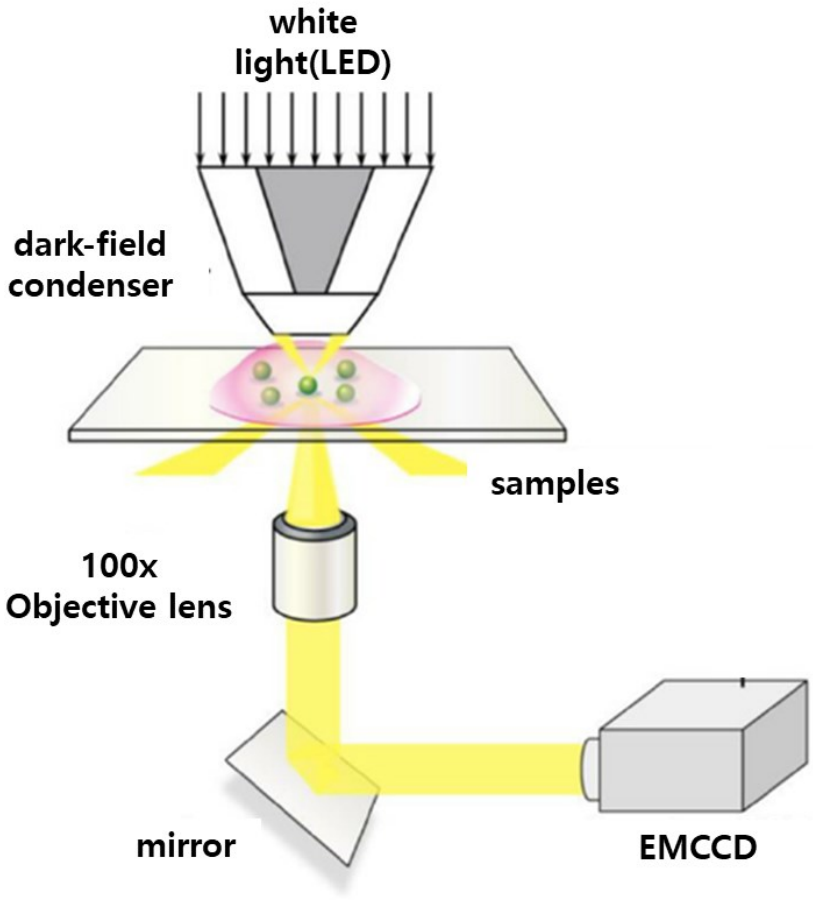

Fig. S3 Schematic to show the working principle of scattering-based DF microscopy and spectroscopy

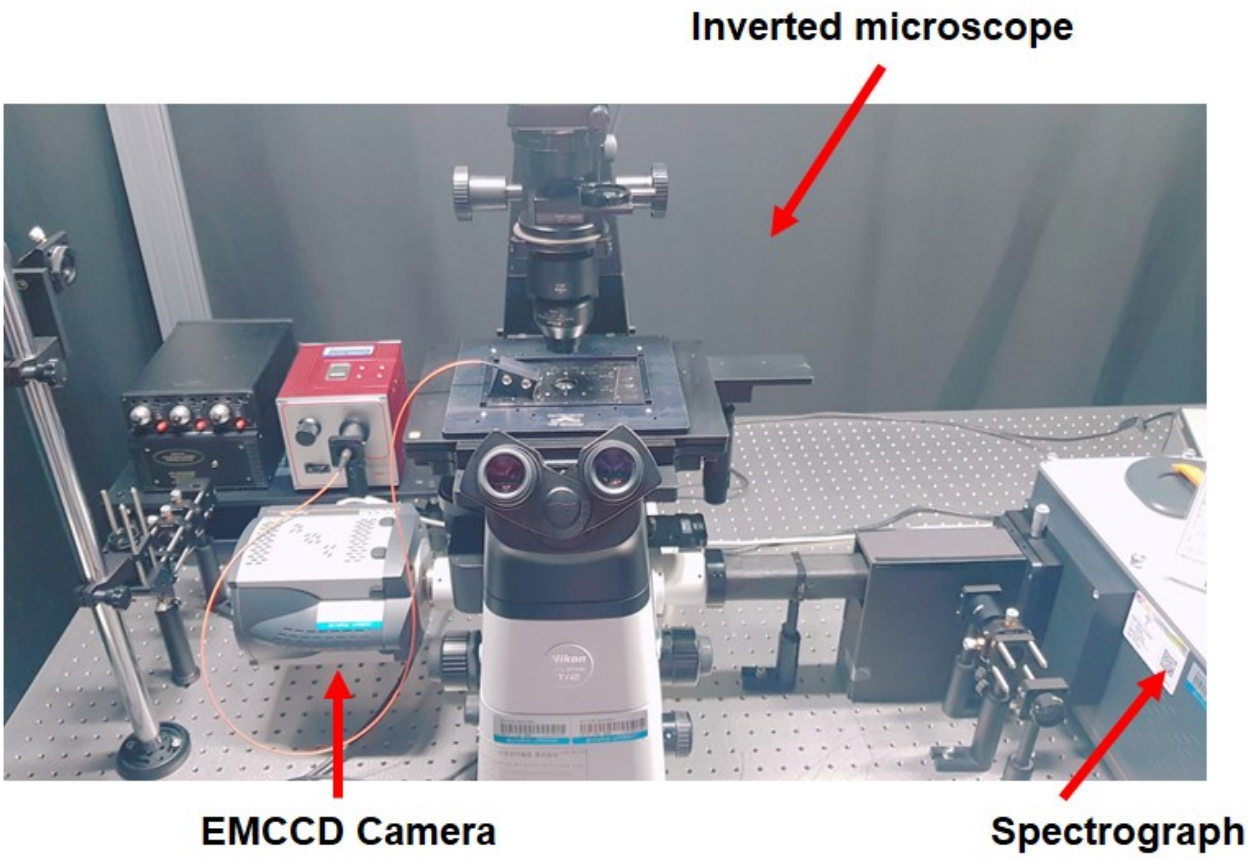

Fig. S4 A photograph to show the experimental setup for single-particle DF microscopy and spectroscopy.

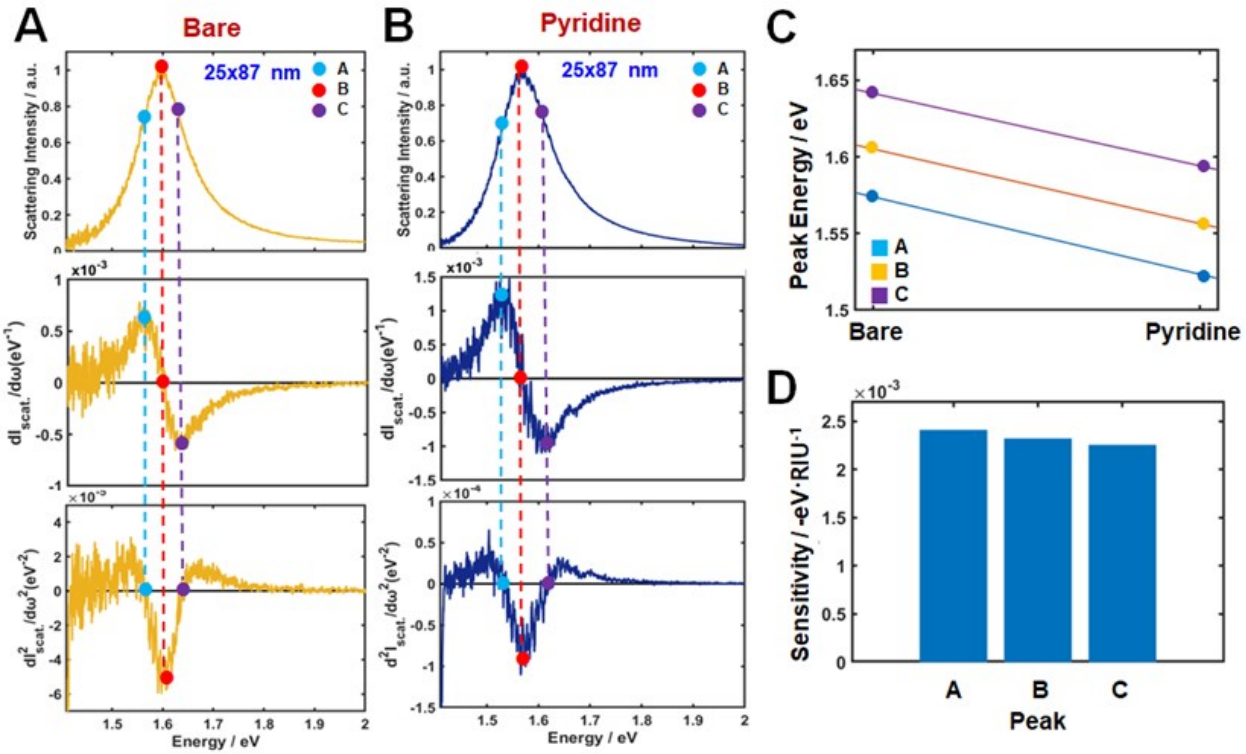

Fig. S5 Inflection point method for single-particle LSPR scattering sensing with AuNRs (25 nm × 87 nm, AR = 3.48) in the presence of the pyridine in water. **(A, B)** LSPR scattering efficiencies (first row), and its first (second row), and second (third row) order derivatives. **(C)** Peak energy plotted against the chemical adsorption of pyridine for points A, B, and C. **(D)** Detection sensitivity on peak shifts A, B and C.

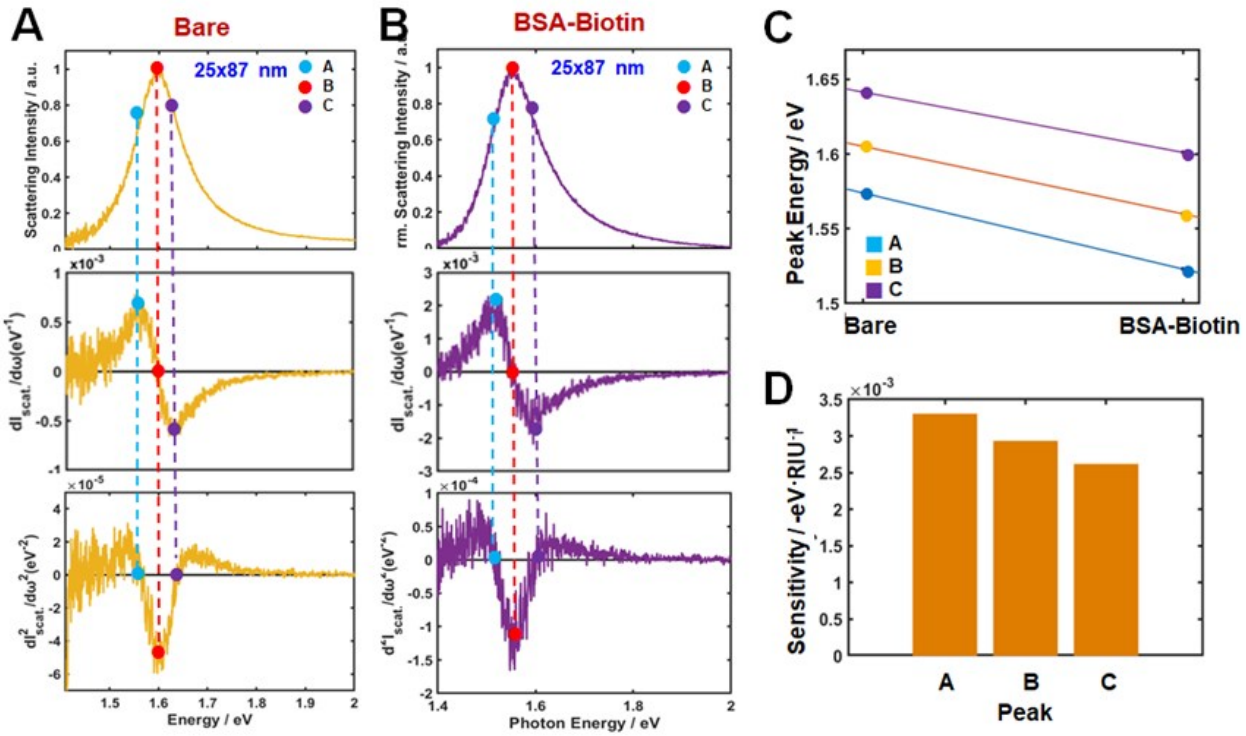

Fig. S6 Inflection point method for single-particle LSPR scattering sensing with AuNRs (25 nm × 87 nm, AR = 3.48) in the presence of the biotinylated BSA proteins (BSA-biotin) in water. **(A, B)** LSPR scattering efficiencies (first row), and its first (second row), and second (third row) order derivatives. **(C)** Peak energy plotted against the chemical adsorption of BSA-biotin for points A, B, and C. **(D)** Detection sensitivity on peak shifts A, B and C.

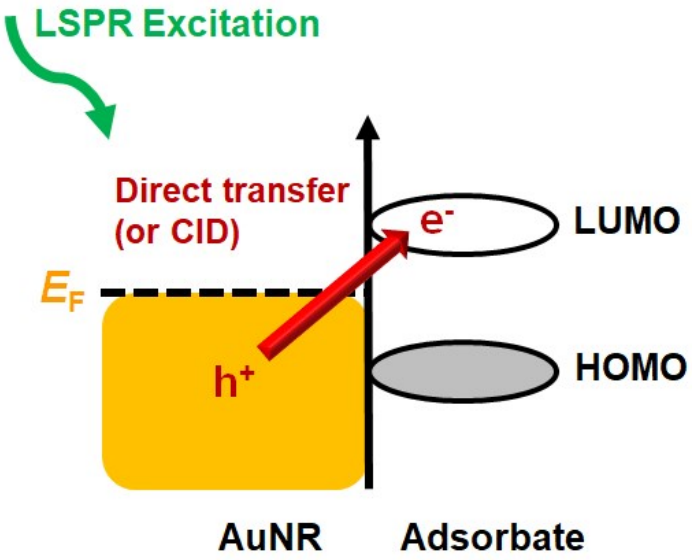

Fig. S7 Schematic depicting the direct interfacial hot-electron transfer (or chemical interface damping) from gold to the LUMO of adsorbate.

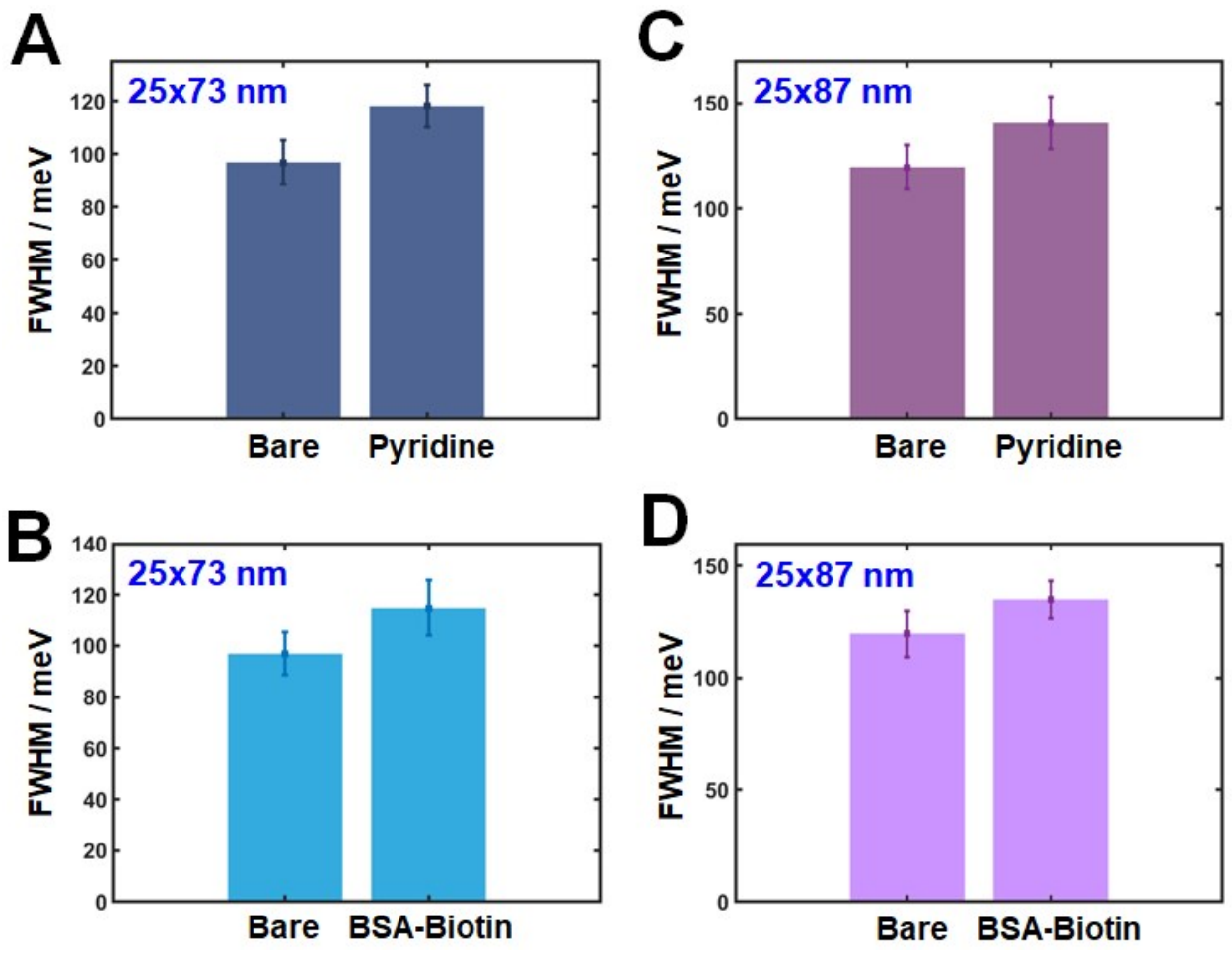

Fig. S8 (A) The LSPR linewidth broadening (or the increase in FWHM) caused by the adsorption of pyridine on the AuNR surface (25 nm × 73 nm). **(B)** The LSPR linewidth broadening caused by the adsorption of BSA-biotin on the AuNR surface (25 nm × 73 nm). **(C)** The LSPR linewidth broadening caused by the adsorption of pyridine on the AuNR surface (25 nm × 87 nm). **(D)** The LSPR linewidth broadening caused by the adsorption of BSA-biotin on the AuNR surface (25 nm × 87 nm).

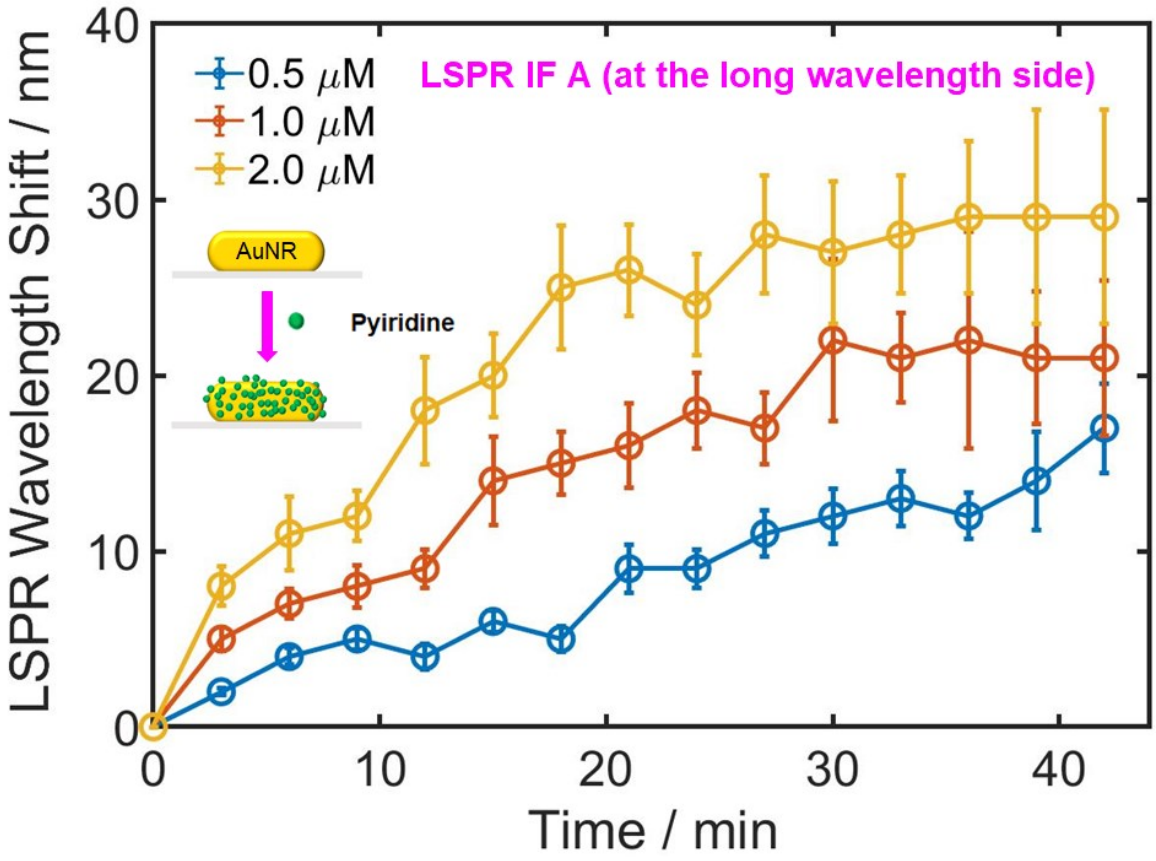

Fig. S9 Effect of the pyridine concentration on the LSPR wavelength shift at the LSPR IF A (longer wavelength side) of single AuNRs (25 nm × 73 nm) in real-time pyridine binding experiments. Scattering spectra of the AuNRs deposited on a glass substrate were obtained as a function of time after adding pyridine with different concentration of 0.5 μM (blue), 1 μM (red), and 2 μM (yellow) in water.